Biochimica et Biophysica Acta 1813 (2011) 1014–1024

Contents lists available at ScienceDirect

Biochimica et Biophysica Acta

journal homepage: www.elsevier.com/locate/bbamcr

Microglial calcium signal acts as a rapid sensor of single neuron damage *in vivo* ☆

Gerhard Eichhoff, Bianca Brawek, Olga Garaschuk *

Institute of Physiology II, University of Tübingen, Keplerstr. 15, 72074 Tübingen, Germany

ARTICLE INFO

Article history:
Received 15 September 2010
Received in revised form 13 October 2010
Accepted 25 October 2010
Available online 5 November 2010

Keywords:
Two-photon microscopy
Calcium imaging
Resting microglia
ATP
Isolectin B4
CX_3CR1

ABSTRACT

In the healthy adult brain microglia, the main immune-competent cells of the CNS, have a distinct (so-called resting or surveying) phenotype. Resting microglia can only be studied *in vivo* since any isolation of brain tissue inevitably triggers microglial activation. Here we used *in vivo* two-photon imaging to obtain a first insight into Ca^{2+} signaling in resting cortical microglia. The majority (80%) of microglial cells showed no spontaneous Ca^{2+} transients at rest and in conditions of strong neuronal activity. However, they reliably responded with large, generalized Ca^{2+} transients to damage of an individual neuron. These damage-induced responses had a short latency (0.4–4 s) and were localized to the immediate vicinity of the damaged neuron (<50 μm cell body-to-cell body distance). They were occluded by the application of ATPγS as well as UDP and 2-MeSADP, the agonists of metabotropic P2Y receptors, and they required Ca^{2+} release from the intracellular Ca^{2+} stores. Thus, our *in vivo* data suggest that microglial Ca^{2+} signals occur mostly under pathological conditions and identify a Ca^{2+} store-operated signal, which represents a very sensitive, rapid, and highly localized response of microglial cells to brain damage. This article is part of a Special Issue entitled: 11th European Symposium on Calcium.

1. Introduction

Microglia are the resident immune cells of the CNS. They play a critical role in defending the structural and functional integrity of the central nervous system [1,2]. In turn, the CNS microenvironment critically impacts on phenotype of resting microglia [2]. In the healthy adult brain, these cells have a small cell body with several long, highly ramified processes, which are used for an active screening/palpation of their immediate neighborhood [3,4]. Because of this ability to actively survey their microenvironment, the microglia in the healthy CNS are often referred to as surveillant microglia. The phenotype of surveillant microglia is often termed "downregulated" because of a limited number of expressed surface molecules as well as their low expression levels [2]. An appearance of a pathological agent/event rapidly initiates a process of microglial activation. When activated, microglia change their morphology, upregulate a number of surface molecules, start secreting inflammatory mediators, and, finally, acquire the features of cytotoxic, phagocytic cells [1,5,6].

Microglia strongly rely in their function on intracellular calcium signaling. *In vitro* data have identified more than twenty ligands of various ionotropic and metabotropic receptors able to evoke receptor-mediated Ca^{2+} signals in microglia (reviewed in [7,8]). In addition, increases in the intracellular free Ca^{2+} concentration ($[Ca^{2+}]_i$) can be induced by activation of store-operated Ca^{2+} channels [8–11] or by Na^+/Ca^{2+} exchangers operating in a reverse mode [12]. *In vitro* studies have suggested that elevations of $[Ca^{2+}]_i$ play a central role in the process of microglial activation (for a review, see [6,8,13,14]). Such Ca^{2+} elevations can be evoked by (i) lipopolysaccharides (endotoxins of the gram-negative bacteria [15]), (ii) purines and pyrimidines, as well as (iii) glutamate and (iv) the chemokine fractalkine released from injured cells (reviewed in [6,10,14,16,17]), (v) amyloidogenic substances accumulating in the brain in the course of a neurodegenerative disease (e.g., amyloid β [18,19]), etc. These receptor-mediated Ca^{2+} signals were shown to control executive functions of activated microglia such as release of trophic factors, NO as well as proinflammatory cytokines and chemokines [1,6,8,14,15].

It remains, however, unclear to what extent the data obtained in reduced preparations (cell cultures (see above)) and brain slices [20]) reflect the properties of surveillant microglia under normal physiological conditions. In *ex vivo* preparations, microglia almost invariably appear at different stages of activation, characteristic of pathology. This is because the isolation of brain tissue is accompanied by a tissue damage, which releases a host of substances triggering microglial activation. Furthermore, cell culture procedures often utilize the tissue from early neonatal brain, where invading microglia are still amoeboid and have not yet been transformed into a differentiated form found in the mature CNS [8,21,22]. Therefore, the mechanisms underlying Ca^{2+} signaling in adult surveillant microglia remained largely unknown.

Here we combined *in vivo* two-photon imaging with several cell-labeling techniques to monitor intracellular Ca^{2+} levels in cortical microglia. Our data show that surveillant microglia rarely generate

☆ This article is part of a Special Issue entitled: 11th European Symposium on Calcium.

* Corresponding author. Tel.: +49 7071 29 73640; fax: +49 7071 29 5395.
E-mail address: olga.garaschuk@uni-tuebingen.de (O. Garaschuk).

0167-4889/$ – see front matter © 2010 Elsevier B.V. All rights reserved.
doi:10.1016/j.bbamcr.2010.10.018

spontaneous Ca^{2+} transients at rest or in conditions of strong neuronal activity but utilize Ca^{2+} release from the intracellular Ca^{2+} stores to signal a focal destruction of a single cell in its vicinity.

2. Materials and methods

All experimental procedures were performed in accordance with institutional animal welfare guidelines and were approved by the government of Baden-Württemberg, Germany.

2.1. In vivo two-photon imaging

Cells in the cortical layers 1–3 (80–160 μm below the cortical surface) were imaged by means of two-photon microscopy in heterozygous *CX$_3$CR1$^{GFP/+}$*, homozygous *CX$_3$CR1$^{GFP/GFP}$*, and wild-type (C57BL/6) mice. Surgery was performed as described in Refs. [23,24]. Briefly, the mice were placed onto a warming plate (38 °C) and anesthetized by inhalation of 1.5% isoflurane (Curamed, Karlsruhe, Germany) in pure O_2. The depth of anesthesia was assessed by monitoring the tail-pinch reflex and respiration rate. After removing the skin, the skull was gently thinned under a dissecting microscope using dental drills. The custom-made recording chamber with a hole in the middle [24] was then glued to the skull with cyanoacrylic glue (UHU, Buhl-Baden, Germany). The mouse was transferred to the setup, placed onto a warming plate (38 °C), and continuously supplied with 0.8–1.2% isoflurane in pure O_2. If necessary, the concentration of isoflurane was adjusted in the course of an experiment in order to keep a rather superficial level of anesthesia (respiration rates between 90 and 120 breaths per minute [25,26]). The recording chamber was perfused with warm (37 °C) extracellular perfusion saline containing (in mM) 125 NaCl, 4.5 KCl, 26 $NaHCO_3$, 1.25 NaH_2PO_4, 2 $CaCl_2$, 1 $MgCl_2$, 20 glucose, pH 7.4, when bubbled with 95% O_2 and 5% CO_2. A craniotomy (~1 mm) was performed above an area devoid of big blood vessels using a thin (30 G) syringe needle.

Two-photon imaging was performed with a custom-built two-photon laser-scanning microscope based on a mode-locked laser operating at 690- to 1040-nm wavelength (MaiTai HP DeepSee, Spectra Physics, Mountain View, CA) and a laser-scanning system (Olympus Fluoview 1000, Olympus, Tokyo, Japan) coupled to an upright microscope (BX61WI, Olympus, Tokyo, Japan) and equipped with a water-immersion objective (40×, 0.80 NA or 60×, 1.0 NA, Nikon, Tokyo, Japan). Enhanced green fluorescent protein (GFP) was excited at a wavelength of 930 nm, whereas Oregon green BAPTA 1 (OGB-1), Fluo-4, and Alexa Fluor 594 (AF 594) were excited at 800 nm. To separate the GFP fluorescence, we used excitation splitting making use of the fact that GFP is very efficiently excited at 930 nm but not at 800 nm [27]. The emitted light was further separated using a beamsplitter either at 515 nm (to separate GFP from the other dyes) or at 570 nm (to separate all dyes from AF 594). Most images were collected at a sampling rate of 4 frames/s. For simultaneous imaging of microglia, astrocytes, and neurons (e.g., Fig. 2C), a sampling rate of 10 frames/s was used. For determination of rise times and latency of microglial calcium transients caused by cell damage, the sampling rate was further increased to 20 frames/s. Unless otherwise indicated, all images shown are maximum intensity projections of ±3–5 μm, taken with a 1-μm step. The microphotographs shown in Figs. 1D, 3C, and 5C represent single-plane images.

Neurons and astrocytes were stained either with OGB-1 (e.g., Fig. 2C) or with Fluo-4 (e.g., Fig. 2A, both from Molecular Probes, USA) using multi-cell bolus loading technique (MCBL [23]). Briefly, the dyes (in the AM (acetoxymethylester) form) were dissolved in DMSO containing 20% Pluronic F-127 (w/v) to a concentration of 10 mM. The injection pipette was pulled using a standard protocol for patch-clamp electrodes (tip diameter 1 μm) and filled with the standard pipette solution of the following composition (in mM): 150 NaCl, 2.5 KCl, and 10 HEPES, pH 7.4, supplemented with 0.5 mM of Ca^{2+} indicator dye. The pipette was placed over the craniotomy and inserted into the brain. When the pipette reached the desired depth of 200 μm, the dye was pressure-ejected into the brain by applying a positive pressure (60 kPa for 2 min). Following dye ejection, the pipette was removed and the experiment commenced about half an hour later. Under these experimental conditions, Fluo-4 predominantly accumulated in astrocytes leaving neurons virtually unstained (see also Refs. [28,29]). In contrast, OGB-1 provided good staining of both neurons and astrocytes [24,30]. In such preparations, astrocytes were identified by their bright appearance [23,30], as well as their cell-type-specific morphology [24].

2.2. In vivo staining of microglia with isolectin B4

The isolectin B4 (IB4) from *Griffonia simplicifolia* seeds has been described as a microglial marker *in situ* [31,32]. For *in vivo* labeling of microglia with IB4, we slightly modified the MCBL protocol. We used Isolectin B4 conjugated to Alexa Fluor 594 (Molecular Probes, USA). To prepare the stock solution, we diluted the dye to a concentration of 500 μg/ml in the standard pipette solution (see above) supplemented with 0.1 mM $CaCl_2$. Frozen aliquots of the stock solution were stored at −20 °C. Immediately before staining, the stock solution was further diluted in the standard pipette solution to gain the final isolectin B4 concentration of 75 μg/ml. This solution was then injected (duration of application: 1.5 min; application pressure: 60 kPa) 200 μm under the cortical surface. This protocol allowed visualization of microglial cells (e.g., Fig. 1B) up to a depth of 300 μm. Besides microglia, Isolectin B4 also labeled endothelial cells of blood vessels, but these long tubular structures were easily distinguished from the microglia (see Fig. 1B).

2.3. In vivo labeling of microglia using single-cell electroporation technique

Microglial cells were stained with OGB-1 hexapotassium salt (Molecular Probes, USA) by means of single-cell electroporation [33]. Briefly, an electroporation pipette (tip diameter <1 μm) was filled with 10 mM OGB-1 dissolved in a solution containing (in mM) 140 K-Gluconate, 14 KCl, 4 NaCl, and 10 HEPES, pH 7.3. A GFP- or AF594-conjugated IB4-labeled microglial cell was targeted by the pipette. As soon as the pipette touched the microglial cell membrane, a negative current of 600 nA was applied for 10 ms using a MVCS-C-01 iontophoresis system (NPI Electronic, Tamm, Germany). After staining, the pipette was immediately withdrawn. Please note that this electroporation protocol is more gentle than those applied *in vivo* to electroporate neurons [33–36]. It allowed clear visualization of all microglial cell somata. Sometimes, however, the OGB-1 signal was too faint to enable visualization of tiny distal processes.

2.4. Drug application

Following pharmacological substances were used in this study: ATP, ATPγS (Adenosine 5′-O-(3-thiotriphosphate)), α-β-MeATP (α,β-methylene-ATP), Bz-ATP (Benzoylbenzoyl-ATP), 2-MeSATP (2-methylthioATP), 2-MeSADP (2-methylthioADP), UDP (Uridine 5′-diphosphate), carbachol, oxotremorine, glutamate, suramin, RB-2 (reactive blue 2), PPADS (pyridoxal-5′-phosphate-6-azophenyl-2′,4′-disulfonic acid), bicuculline (all obtained from Sigma-Aldrich, St. Louis, MO, USA); trans-ACPD ((±)-1-aminocyclopentane-trans-1,3-dicarboxylic acid), thapsigargin (obtained from Tocris, Bristol, United Kingdom); Fractalkine (Recombinant Mouse CX_3CL1 Chemokine Domain, obtained from R&D systems, Minneapolis, MN, USA); KCl (solution contained (in mM): 80 KCl, 50 NaCl, 1.25 NaH_2PO_4, 26 $NaHCO_3$, 2 CaCl, 1 MgCl, pH 7.4 when bubbled continuously with 95% O_2 and 5% CO_2).

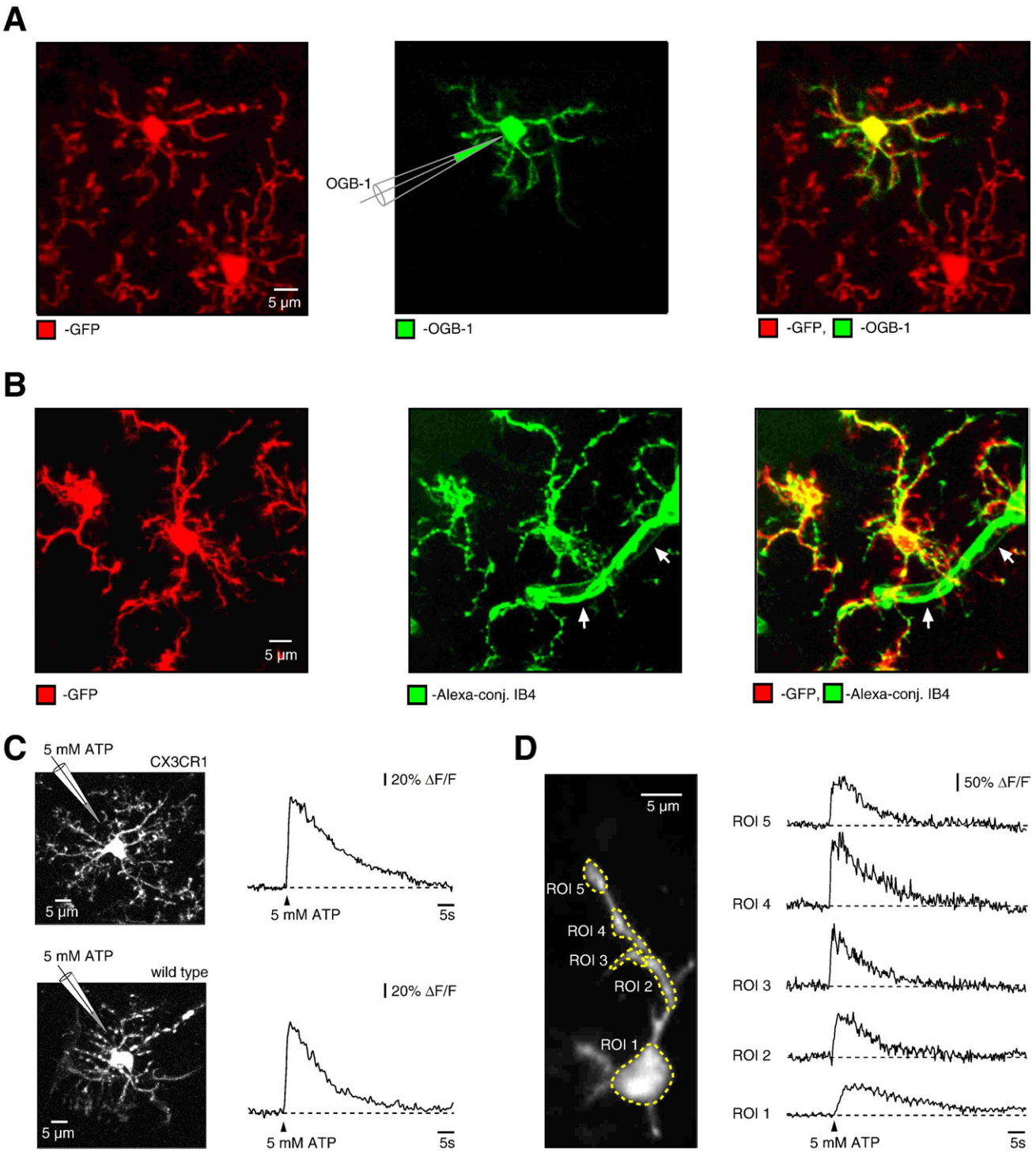

Fig. 1. *In vivo* calcium imaging of microglial cells. (A) *In vivo* labeling of microglial cells with Ca^{2+} indicator dye OGB-1. Left: a micrograph of GFP-positive microglial cells in a $CX_3CR1^{GFP/+}$ mouse. Middle: the upper microglial cell is stained with OGB-1 using a single-cell electroporation technique (electroporation pulse: 10 ms, −600 nA). Schematic drawing indicates the position of electroporation pipette filled with 10 mM OGB-1. Right: an overlay of the left and the middle images. (B) Left: an image of microglial cells in a $CX_3CR1^{+/GFP}$ mouse. GFP fluorescence is excited at 930 nm, emitted light is sampled between 420 and 515 nm. Middle: the same cells imaged after staining with Alexa Fluor 594-conjugated Isolectin B4 using MCBL (excited at 800 nm, emitted light is sampled between 515 and 725 nm). Right: an overlay of the two images. Note that isolectin B4 stains blood vessels (arrows) in addition to microglia. Microphotographs shown in panels A and B represent maximum intensity projections of image stacks (± 10 µm, step 1 µm). (C) Somatic microglial Ca^{2+} transients in CX_3CR1 (top) and wild-type (bottom) mice evoked by 5 mM ATP (applied locally by pressure injection, 50 ms, 20 kPa). (D) ATP-evoked Ca^{2+} transients recorded in the soma and in the processes of a microglial cell. The corresponding regions of interest (ROIs) are marked with respective numbers on the left panel.

The substances were either applied topically (e.g., added to the extracellular saline perfusing the chamber attached to the mouse's skull [24,37]) or locally (by pressure ejection, using a pressure-ejection system from NPI Electronic, Tamm, Germany) directly to the cells of interest. Locally applied drugs were dissolved (except of fractalkine) in the standard pipette solution (see above). The chemokine domain of fractalkine was dissolved in PBS containing 0.1% bovine serum albumin (both obtained from Invitrogen GmbH, Karlsruhe, Germany) to a final concentration of 250 µg/ml.

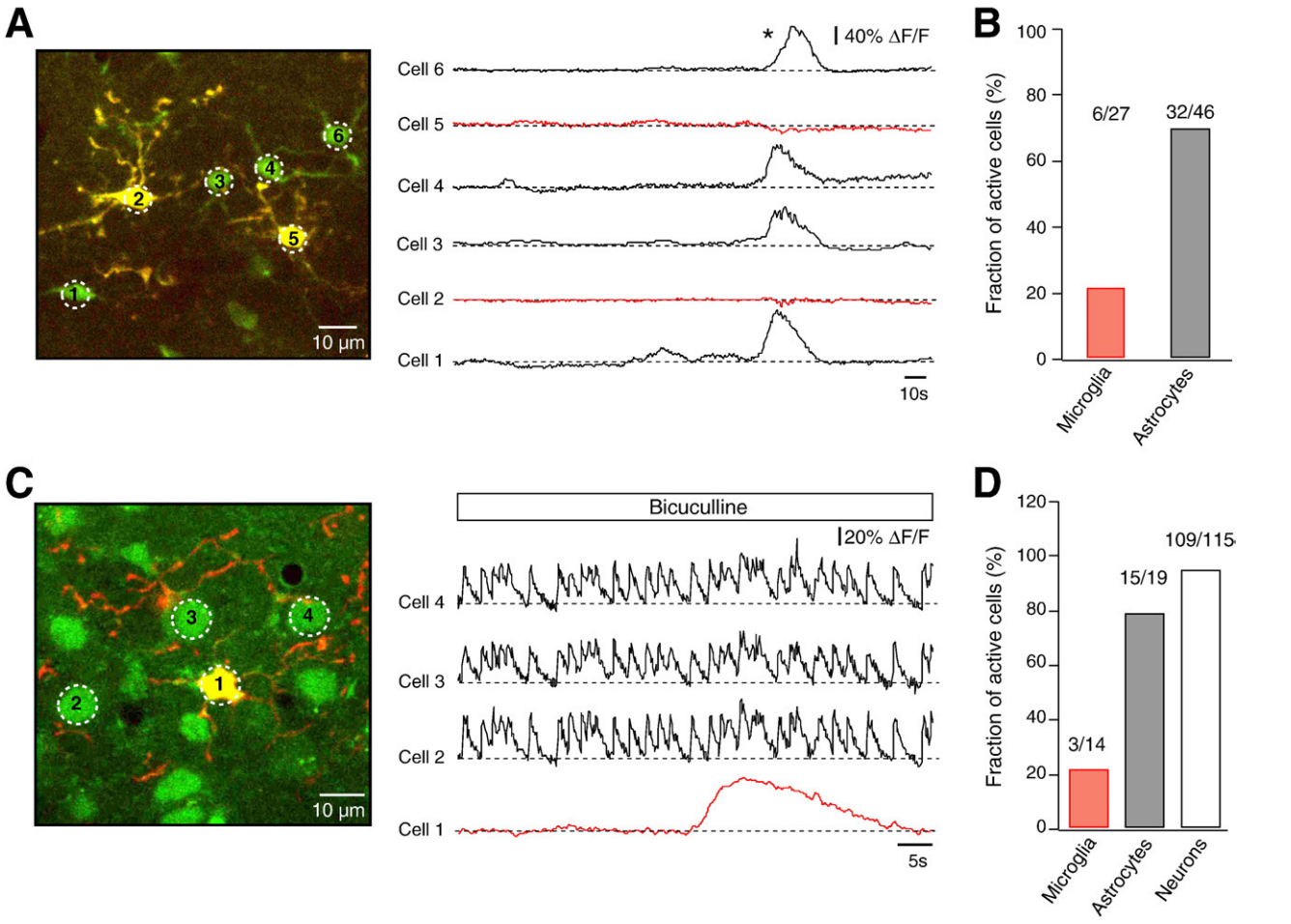

Fig. 2. Spontaneous calcium signals in microglia. (A) Continuous recordings of $[Ca^{2+}]_i$ (right) in astrocytes (black traces) and microglia (red traces), marked with respective numbers in the left panel. GFP-positive microglial cells (red) were labeled with OGB-1 (green) and therefore appear yellow. Astrocytes were stained with Fluo-4 (green) using MCBL. Asterisk indicates an intercellular astrocytic Ca^{2+} wave. (B) A bar graph illustrating the fraction of cells showing a spontaneous Ca^{2+} transient during a 15-min-long recording period. (C) Simultaneous recordings of $[Ca^{2+}]_i$ in the microglia (red trace), and in layer 2/3 cortical neurons (black traces) during a period of increased neuronal activity caused by a topical application of the $GABA_A$ receptor antagonist bicuculline (250 µm). The corresponding cells are marked with the respective numbers in the left panel. The GFP-positive microglial cell (red) was stained with OGB-1 (green) via electroporation and therefore appears yellow. Neurons and astrocytes were loaded with OGB-1 using MCBL and discriminated based on their characteristic shape and on the brightness of their staining [23]. (D) A bar graph showing the fraction of cells active during bicuculline application.

To allow visualization of the drug application pipette and to improve the precision of the pipette positioning, 50 µM of the cell-impermeant, red fluorescent dye Alexa Fluor 594 (AF 594, Molecular Probes, Eugene, Oregon, USA) was added to the drug-containing solution in some experiments. The application pipette (tip diameter 1 µm) was placed under the visual control 30 to 40 µm away from the microglial cell of interest and a pressure pulse of 20–35 kPa was applied for 50 ms. Successful drug application was ascertained either by fluorescence of AF 594 or by the small (~1–3 µm) movement artifact caused by the pressure application (e.g., Fig. 5C).

The blockers of P2-purinoceptors (suramin, RB-2, PPADS) were pressure applied directly to the recorded microglial cell at continuous pressure of 4 kPa. Application started at least 1 min before damaging a neuron (see below). Prolonged application of some blockers (e.g., RB-2) resulted in darkening of the recorded area and disappearance of microglial processes. Therefore, we did not increase the blocker's concentration further. A similar protocol was used in occlusion experiments (e.g., Fig. 5A and B) for the application of ATPγS, UDP and 2-MeSADP. Finally, thapsigargin (25 µM) was also applied directly to the microglial cell of interest by five repetitive pressure pulses (50 ms, 35 kPa). Bicuculline (250 µM) was applied topically for 20 min preceding the recordings and was present in the extracellular saline throughout the experiment.

2.5. Cell damaging procedure

A micropipette was filled with the extracellular perfusion saline (see above) supplemented with 500 µM of Alexa Fluor 594 (the resistance of the filled pipette: 6–7 MOhm). Thereafter, the pipette was positioned into the layer 2/3 at a desired distance from the microglial cell of interest within the same imaging plane. A minimal positive pressure was applied to the pipette to release small amount of AF 594 into the extracellular space. This procedure allowed visualizing the soma of a nearby cortical layer 2/3 neuron as a negative image [36]. Thereafter, the cell-damaging pipette was positioned at the cell membrane and rapidly moved forward by 10 µm in a step-like fashion while imaging the microglial cell. Upon the rupture of the cell membrane, the resistance of the micropipette (continuously monitored with MVCS-C-01 M-45 unit; NPI electronic, Tamm, Germany) dropped from approximately 12–13 MOhm (when touching the cell membrane) back to 6–7 MOhm and Alexa Fluor 594 diffused into the neuron (e.g., Fig. 3A). The time point of neuronal damage was estimated either from an increase in the fluorescence within a region of interest positioned inside the

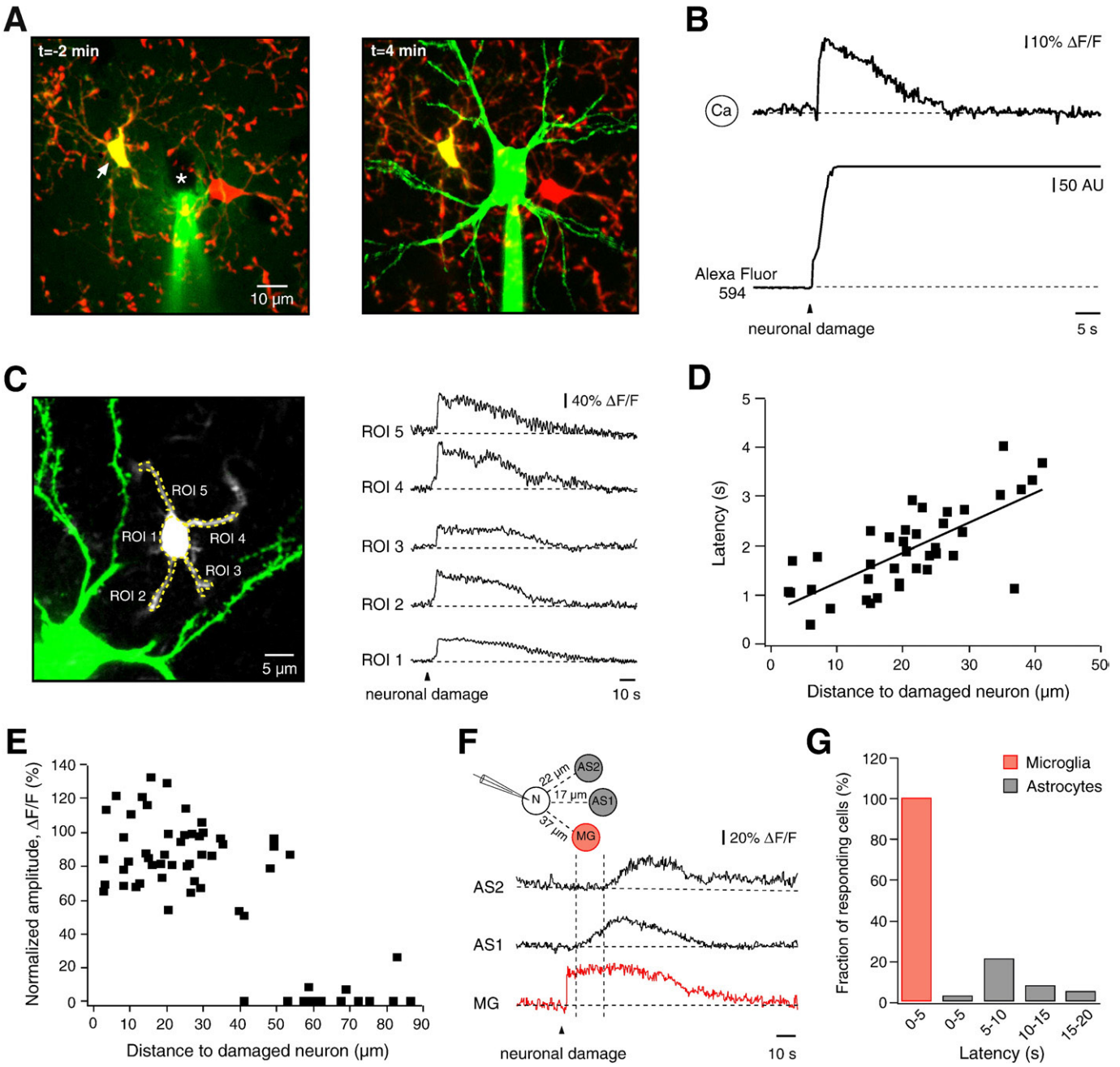

Fig. 3. Neuronal damage causes rapid Ca^{2+} signals in microglial cells. (A) Maximum intensity projections (±15 µm) taken 2 min before (left) and 4 min after (right) the cell damaging procedure (described in detail in Materials and methods). Left: two GFP-positive microglial cells are shown in red; the left one (arrow) is stained with OGB-1 (green) and therefore appears yellow. The cell-damaging pipette filled with AF 594 (green) is touching a neuron (seen as a dark shadow, asterisk). Note that after the rupture of the cell membrane, the neuron was immediately filled with AF 594, diffusing out of the pipette (right). (B) A recording of microglial $[Ca^{2+}]_i$ (top) and of the intraneuronal AF 594 fluorescence (bottom). Alexa fluorescence is recorded from the region of interest located within the targeted (and later damaged) neuron. The time point of neuronal damage is identified as the time point at which Alexa fluorescence starts to increase within the targeted neuron (arrowhead in B). (C) DICTs (right) recorded from regions of interest marked with respective numbers in the left panel. The microglia is stained with OGB-1 (grayscale single-plane image) and the damaged cell is filled with AF 594 (green). (D) Dependence of the DICT latency on the soma-to-soma distance (from the border of one cell soma to the border of the other) between the microglia and the damaged neuron. The solid line represents the linear least squares fit to the data. (E) DICT amplitudes (normalized to the amplitude of the Ca^{2+} transient induced in the same cell by 5 mM ATP) plotted against the corresponding soma-to-soma distances between the microglia and the damaged cells. (F) Simultaneous recordings of $[Ca^{2+}]_i$ in microglia and neighboring astrocytes (located as illustrated in the inset). (G) A bar graph illustrating the fraction of microglial cells (red, $n=50$) and astrocytes (gray, $n=1, 8, 3, 2$, total of 14 cells) responding to neuronal damage with a given latency.

damaged cell (e.g., Fig. 3B) or from the drop in the pipette resistance. For quantitative measurements (e.g., estimating the latencies of damage-associated Ca^{2+} transients, Fig. 3D), the latter, more precise method was used. In was possible to repeat this experiment several times by killing neurons at different distances from the microglial cell of interest.

2.6. Image analyses

Image analyses were performed off-line with the *ImageJ* software (http://rsb.info.nih.gov/ij/) and *Igor Pro* (Wavemetrics, Lake Oswego, Oregon, United States). Measured values are given as mean ± SEM.

3. Results

3.1. In vivo calcium imaging of microglial cells

Functional properties of resting microglia were studied in the cortex of adult (2- to 4-month-old) mice using high-resolution *in vivo* two-photon imaging. To visualize microglial cells, we first used heterozygous *CX$_3$CR1*$^{+/GFP}$ mice (*CX$_3$CR1 mice* [38]) in which the *CX$_3$CR1* gene in the mutant allele is replaced by a gene coding for the enhanced green fluorescent protein (GFP). Because multi-cell bolus loading technique (MCBL [23]) usually produces a very poor staining of microglia (Supplementary Fig. 1), we stained microglial cells with the Ca^{2+} indicator dye Oregon green BAPTA 1 (OGB-1) using a single-cell electroporation technique (Fig. 1A, see Materials and methods for details). In addition, we used wild-type (WT) mice in this study. Microglia in WT mice were identified by their ability to bind a glycoprotein isolectin B4 [31,32]. As shown in Fig. 1, an MCBL-like injection of isolectin B4 conjugated with a red dye Alexa Fluor 594 (AF 594; see Materials and methods for details) brightly stained microglia (and blood vessels) in *CX$_3$CR1* and WT mice. The AF 594-labeled cells were subsequently electroporated with OGB-1 as described above.

Several lines of evidence suggested that the electroporation protocol used did not harm the functional properties of microglial cells. First, after electroporation, OGB-1-labeled microglia preserved their ramified morphology for at least an hour, which was an average duration of our recordings (Supplementary Fig. 2A; $n=8$ cells monitored on average for 62.5 ± 5.6 min). Second, we analyzed the chemotactic response [4] of labeled cells. As illustrated in Supplementary Fig. 2B, the cells preserved the capability of directed process extension towards the tip of an ATP-containing pipette. Only in about 10% of cases, the entire cell turned extremely bright immediately after electroporation and its processes became fragmented, indicating cell damage. These cells were excluded from further analyses.

To compare the strength of the chemotactic response of GFP-labeled microglia in *CX$_3$CR1* and AF 594-labeled microglia in WT mice, we measured the diameter of the spherical containment formed by microglial processes around the ATP-containing pipette. Thirty minutes after the pipette insertion, the diameter amounted to 8.3 ± 0.5 μm in WT ($n=18$ trials) and to 9.2 ± 0.3 μm in *CX$_3$CR1* ($n=13$) mice ($p=0.5$, Student's *t*-test).

A brief pressure application of 5 mM ATP triggered large intracellular Ca^{2+} transients in the OGB-1-labeled microglia in both *CX$_3$CR1* and WT mice (Fig. 1C). These Ca^{2+} signals were seen throughout an entire cell including its processes (Fig. 1D). The kinetic properties of ATP-evoked microglial Ca^{2+} transients were similar in *CX$_3$CR1* and WT mice (rise time: 0.8 ± 0.1 s, $n=10$ cells in *CX$_3$CR1* vs. 0.8 ± 0.1 s, $n=10$ cells in WT mice, $p=0.9$, Student's *t*-test; decay time constant: 5.1 ± 0.1 s in *CX$_3$CR1* vs. 6.4 ± 0.8 s in WT mice, $p=0.2$, Student's *t*-test). Other stimuli (see below) also elicited similar Ca^{2+} signals in both mouse strains. Therefore, in the results presented below, the data obtained from both mouse strains have been averaged together.

3.2. Spontaneous Ca^{2+} signaling in microglia

Because ATP can be released under physiological conditions (e.g., from axons and astrocytes [39], it may cause "spontaneous" Ca^{2+} transients in resting microglial cells, as was shown *in vitro* [40]. To test whether this is the case *in vivo*, we simultaneously imaged microglial cells and astrocytes over long periods of time (Fig. 2A). In the course of a 15-min-long recording period, 70% of astrocytes (32/46 cells) showed at least one spontaneous Ca^{2+} transient (mean frequency 0.2 ± 0.1 transients/min) whereas 78% of microglial cells (21/27) remained silent. The remaining 6 cells exhibited Ca^{2+} transients with amplitudes of $40.4\pm6.0\%$ $\Delta F/F$, rise times of 12.4 ± 3.7 s and decay time constants of 12.0 ± 2.1 s ($n=14$ transients). In 4 out of 6 cells, more than a single Ca^{2+} transient was observed. The interval between the two successive transients (from beginning of the first until the beginning of the second) was on average 2.3 ± 0.2 min ($n=7$ intervals).

Next we asked whether microglia participated in so-called intercellular astrocytic Ca^{2+} waves (for a recent review, see [41]), which caused correlated Ca^{2+} increases in surrounding astrocytes (asterisk in Fig. 2A, right). Astrocytic Ca^{2+} transients were considered to belong to the same Ca^{2+} wave if they occurred in all participating cells within ±5-s time window (measured from the Ca^{2+} transient with the median latency). Altogether we have analyzed 45 waves involving two astrocytes, 19 waves involving three, 12 waves involving four and one intercellular Ca^{2+} wave involving five astrocytes. Out of these 77 waves, there was a single case when two microglial cells were active simultaneously with 4 astrocytes (latency from the temporally closest astrocytic Ca^{2+} transient to those in microglia was 1.5 and 2 s, respectively). However, these microglial cells did not participate in the following Ca^{2+} waves involving the same astrocytes (2 waves involving 4 and 2 waves involving 3 astrocytes). The remaining microglial Ca^{2+} transients either occurred completely in the absence of astrocytic activity, or had a very long latency (0.5–1 min) to the temporally closest astrocytic Ca^{2+} transient, with microglial transients both preceding and following the Ca^{2+} transients in astrocytes. We concluded therefore that surveillant microglia do not participate in astrocytic Ca^{2+} waves.

In the next series of experiments, we topically applied $GABA_A$ receptor antagonist bicuculline (see Materials and methods for details) to induce strong neuronal activity and simultaneously imaged neurons, astrocytes, and microglia. Under these conditions, 95% of neurons showed typical synchronized Ca^{2+} transients with a mean frequency of 30–40 transients per minute [42,43]. In addition, we observed an increase in the fraction of active astrocytes (from 70 to 79%; mean frequency 0.2 ± 0.1 transients/min). However, even in conditions of strong neuronal activity, 79% of microglial cells remained silent. Microglial Ca^{2+} transients were seen only in 3 out of 14 recorded cells. These Ca^{2+} transients, however, were somewhat larger and longer than the ones observed under control conditions (amplitudes: $50.7\pm7.7\%$ $\Delta F/F$, rise times: 8.2 ± 1.8 s and decay time constants: 22.0 ± 3.3 s ($n=7$ transients)). Thus, with regard to their Ca^{2+} signaling, the majority of microglial cells are silent both at rest and under conditions of strong neuronal activity.

3.3. Damage-induced microglial Ca^{2+} transients

Next, we tested whether microglia respond with Ca^{2+} signals to damage of an individual neuron. To this end, we filled a micropipette with Alexa Fluor 594, positioned it at the surface of a neuron, and rapidly moved it forward by 10 μm, thereby inserting the pipette into the cell (Fig. 3A; see Materials and methods for details). To ensure that the inserted pipette remained inside the damaged cell and therefore never directly came into contact with microglia, we routinely made 3D reconstructions of the imaged area (Supplementary Movie). This cell-damaging procedure reliably evoked Ca^{2+} transients in all surrounding microglia (Fig. 3B; $n=17$ trials in $n=9$ cells in *CX$_3$CR1* and $n=43$ trials in $n=19$ cells in WT mice). We termed these microglial Ca^{2+} signals the damage-induced Ca^{2+} transients or DICTs. Importantly, no DICTs were observed when the pipette was similarly moved forward in the surrounding neuropil without targeting a neuron (n = 15, not shown). The damage-induced Ca^{2+} transients occurred both in cell bodies and in the microglial processes (Fig. 3C). They had large amplitudes (comparable to those evoked by 5 mM ATP, Fig. 3E) and long durations but relatively short onset latencies (the shortest being 400 ms). The DICT latencies increased linearly with the distance between the damaged neuron and the recorded microglial cell, reaching some 3.5 s at a distance of 40 μm (Fig. 3D).

Surprisingly, the amplitudes of the Ca^{2+} transients remained unchanged over the first 40–50 μm but rapidly decreased thereafter, so that no DICTs were detected in more distant microglia (Fig. 3E). The existence of this sharp border suggests that DICTs are restricted to the microglial cells immediately adjacent to the damaged neuron and that the cell-damage-related signal does not pass to more distantly located microglia.

If the DICTs are caused by a diffusible substance released from the damaged neuron, this substance may also directly signal to neighboring astrocytes. To test this hypothesis, we simultaneously imaged microglia and astrocytes when damaging a neuron (Fig. 3F, G). Out of 37 astrocytes tested, only 16 cells (43%) showed a Ca^{2+} transient during the recording period following the neuronal damage. To distinguish between spontaneous (see Fig. 2A) and damage-related astrocytic Ca^{2+} transients, we compared the percentage of cells active during identical time intervals (i) preceding and (ii) following neuronal damage. The results (Supplementary Fig. 3) suggest that there is a correlation between astrocytic Ca^{2+} transients and neuronal damage. However, the latencies of the astrocytic Ca^{2+} transients were much longer compared to the DICT latencies and did not depend on the distance to the damaged cell (Supplementary Fig. 3B). The average latency of astrocytic Ca^{2+} transients was 34.8 ± 3.6 s ($n = 16$), more than 7 times longer than that of the microglia (Fig. 3D, G; Supplementary Fig. 3B). Taken together, these data show that only microglia reliably respond to neuronal damage with a Ca^{2+} transient.

3.4. Mechanisms underlying the damage-induced Ca^{2+} transients

To understand the mechanisms underlying DICTs, we first determined the pharmacological profile of microglial Ca^{2+} signals *in*

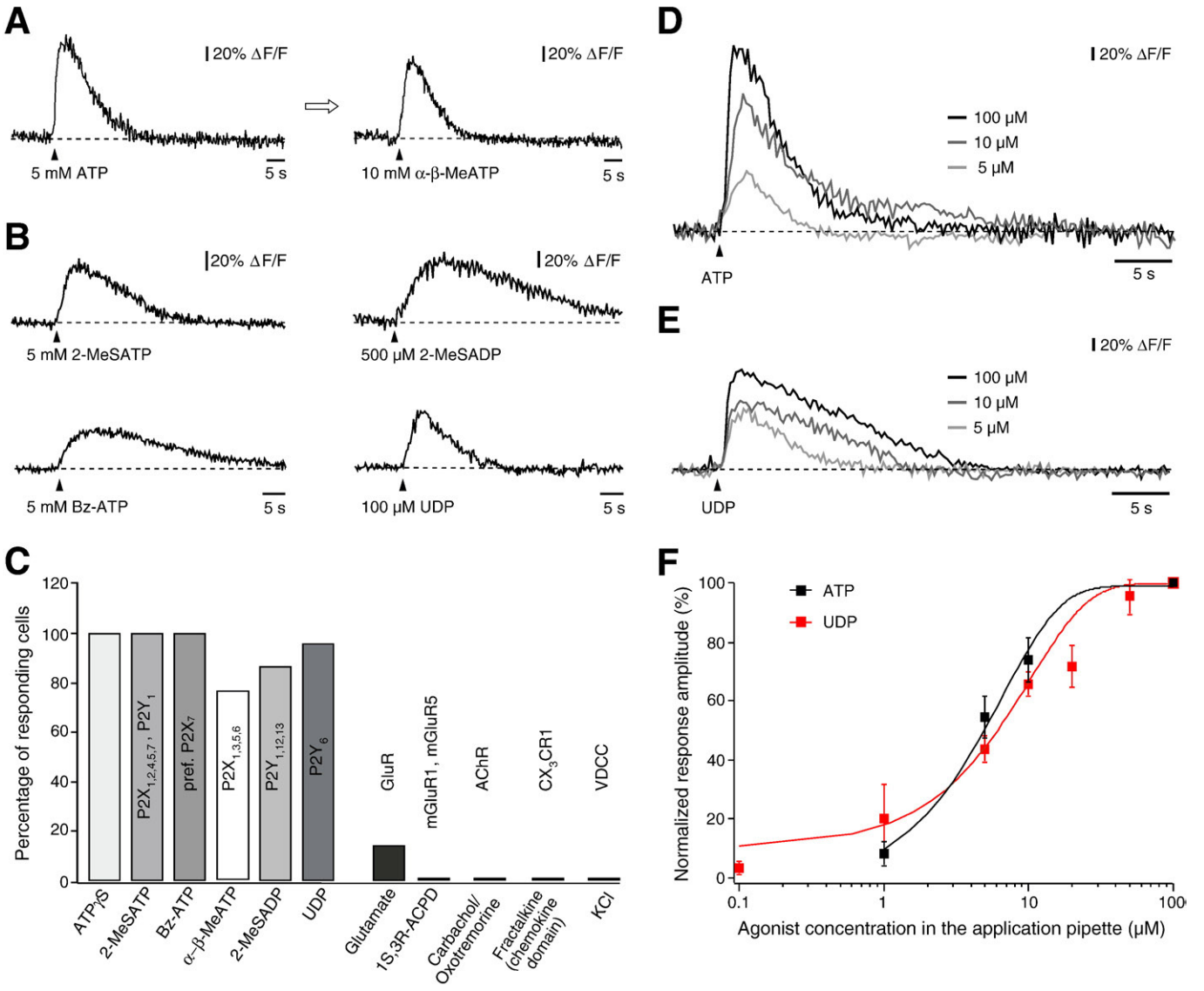

Fig. 4. Pharmacological profile of microglial Ca^{2+} signals. (A) Here and below each cell was first challenged with a brief ATP application (left; 5 mM, 50 ms, 20 kPa) and then with the drug tested (α-β-MeATP (α,β-Methylene-ATP); 10 mM, right). (B) Representative examples of Ca^{2+} transients evoked by 2-MeSATP (2-methylthioATP; 5 mM, top left), 2-MeSADP (2-methylthioADP; 500 μM, top right), Bz-ATP (Benzoylbenzoyl-ATP; 5 mM, bottom left), and UDP (Uridine 5′-diphosphate; 100 μM, bottom right). (C) A bar graph showing the percentage of cells responding with a Ca^{2+} transient to application of a given agonist. From left to right: ATPγS (adenosine 5′-O-(3-thiotriphosphate); 5 mM, $n = 12$); 2-MeSATP (5 mM, $n = 16$); Bz-ATP (5 mM, $n = 42$); α-β-MeATP (10 mM, $n = 13$); 2-MeSADP (500 μM, $n = 51$); glutamate (10 mM, $n = 14$); trans-ACPD ((±)-1-aminocyclopentane-trans-1,3-dicarboxylic acid; 5 mM, $n = 14$); carbachol (10 mM, $n = 7$)/oxotremorine (5 mM, $n = 7$); fractalkine (chemokine domain; 250 μg/ml, $n = 7$) and KCl (80 mM, $n = 5$). Receptors targeted by the respective agonists are listed within the appropriate bar. (D–F) Dose–response relations for two purinergic receptor agonists. Representative responses of microglial cells to increasing concentrations of ATP and UDP are shown in panels D and E, respectively. (F) Dose–response curves for ATP (black, $n = 11$ cells) and UDP (red, $n = 11$ cells). The response amplitude is normalized to the maximum change in fluorescence caused by application of 100 μM ATP or UDP, respectively. Solid lines represent fits to respective sets of data using the Hill equation.

vivo (Fig. 4A–C). In order to do so, each cell was first challenged with ATP and then with one of the agonists of purinergic, cholinergic or glutamatergic receptors, etc. (e.g., Fig. 4A). To exclude unexpected network effects, these experiments were conducted in the presence of 2 μM TTX in the perfusion saline. As summarized in Fig. 4C, microglia readily responded with Ca^{2+} transients to agonists of P2X and P2Y receptors, such as α-β-MeATP (α,β-Methylene-adenosine-5′-triphosphate), Bz-ATP (benzoylbenzoyl-ATP), UDP, etc.

ATP and UDP also evoked clear Ca^{2+} transients when applied at very low concentrations (1–5 μM in the application pipette; Fig. 4D–F). Taking into account the dilution of the drug during its diffusion in the extracellular space (Eq. (17) in [44]), the effective concentration reaching the cell under these conditions is estimated to be in the submicromolar range. Such high sensitivity to ATP is unique to surveillant microglia because cultured microglial cells do not respond to ATP applied in the concentration lower than 10 μM [40]. Responses with the maximal amplitude ($69.22 \pm 6.77\%$ ΔF/F, $n = 10$) were observed at 100 μM ATP in the application pipette (Fig. 4F). Application of 5 mM ATP did not cause any further increase in the response amplitude ($75.26 \pm 3.12\%$ $\Delta F/F$, $n = 30$; not significantly different from that evoked by 100 μM ATP, $p = 0.5$, Student's *t*-test). Thus, Ca^{2+} signaling in resting microglial cells *in vivo* is mediated by purinergic receptors with high agonist sensitivity.

Next we applied glutamate to stimulate ionotropic and metabotropic glutamate receptors known to be expressed by cultured microglia [45]. The application protocol used for studying P2-receptor-mediated signaling (e.g., drug application for 50 ms at 20–35 kPa) caused glutamate-activated Ca^{2+} transients only in 14% of cells (2/14) and failed to produce any *trans*-ACPD-mediated Ca^{2+} signals (Fig. 4C). However, using significantly longer drug applications

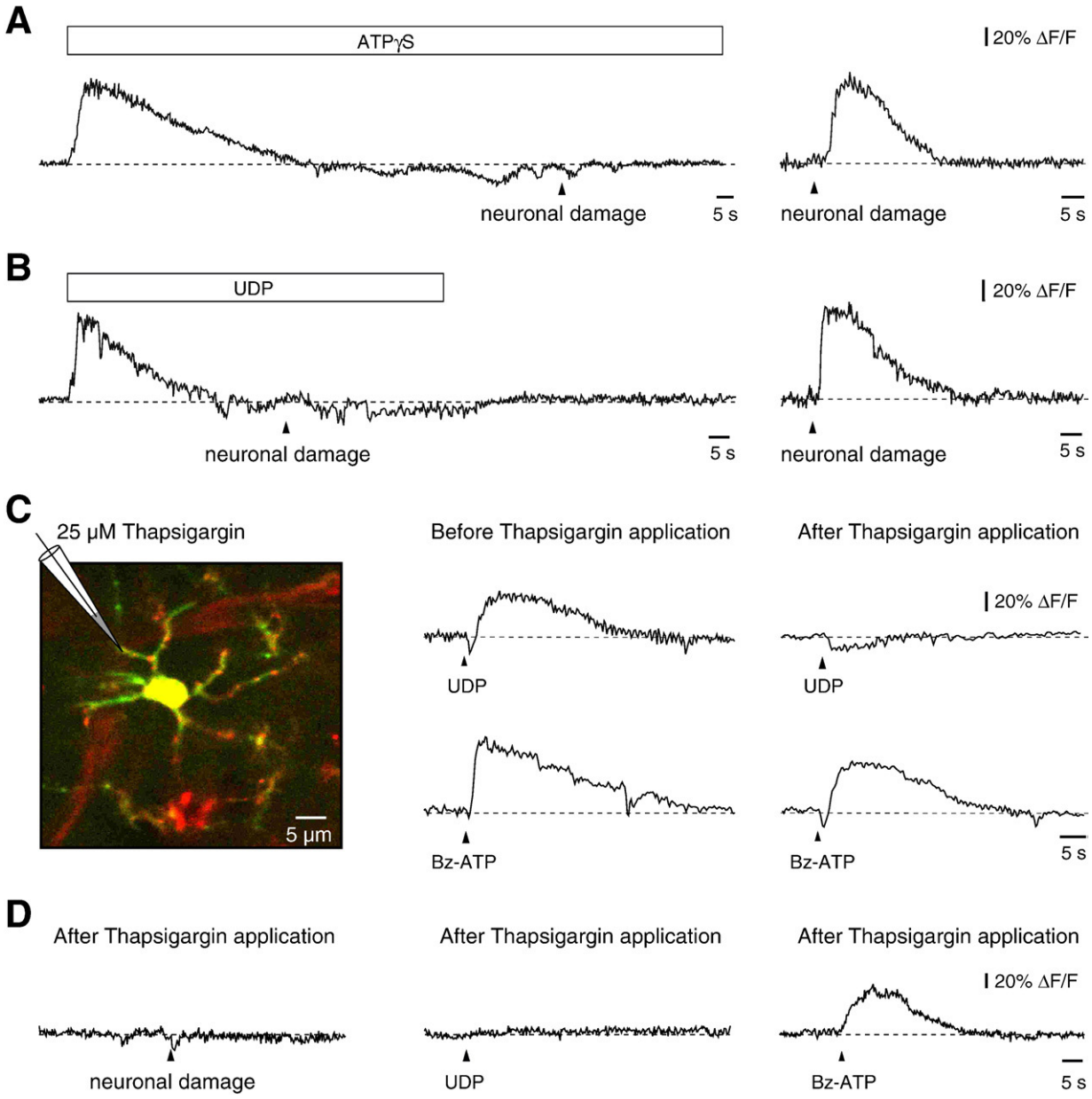

Fig. 5. The mechanism underlying damage-induced Ca^{2+} transients in microglia. (A) $[Ca^{2+}]_i$ recordings from the same microglial cell during (left) and 5 min after (right) local application of 5 mM ATPγS. Note that neuronal damage fails to cause any DICTs during (left) but not after (right) ATPγS application. Two different neurons were damaged in this experiment, one during and one after the application of ATPγS. (B) The same experiment as in panel A using the local application of 100 μM UDP. (C) Microglial Ca^{2+} transients evoked by a brief pressure application of 100 μM UDP (top, middle, and right) and 5 mM Bz-ATP (bottom, middle, and right) before (middle) and after (right) five repetitive 50-ms-long pressure applications of thapsigargin. A single-plane image of the recorded cell is shown in the left panel. (D) A continuous recording of $[Ca^{2+}]_i$ in another microglial cell during neuronal damage (left) as well as UDP (middle) and Bz-ATP (right) applications conducted after the thapsigargin treatment.

(200–300 ms), responses to glutamate were induced in 5 out of 8 cells tested. A smaller fraction (29%; 2/7 cells) responded to prolonged application of the agonist of metabotropic glutamate receptors, *trans*-ACPD. Other drugs/treatments, which were shown to induce microglial Ca^{2+} signals *in vitro* (e.g., cholinergic agonists [46,47], fractalkine [48], and depolarization of the cell membrane [49]), were ineffective (Fig. 4C). Because fractalkine is released by the damaged neuron [50] and theoretically could trigger DICTs, we performed cell-damaging experiments in homozygous $CX_3CR1^{GFP/GFP}$ mice lacking the fractalkine receptor. However, we observed the full-blown DICTs in these mice, too (normalized DICT amplitude (e.g., Fig. 3E) was 0.99 ± 0.03, $n = 4$). These data are consistent with the finding that the soluble form of fractalkine fails to evoke any Ca^{2+} signals in microglia *in vivo* (Fig. 4C) and argue against the role of fractalkine in generating DICTs.

As shown in Fig. 5A and B, DICTs were completely and reversibly occluded by ATPγS ($n = 5$) or UDP ($n = 5$). Continuous applications of ATPγS (5 mM, Fig. 5A) or UDP (100 μM, Fig. 5B) directly to the recorded microglia (see Materials and methods for details) initially caused elevations in $[Ca^{2+}]_i$ themselves. These Ca^{2+} elevations, however, were transient with $[Ca^{2+}]_i$ returning to the baseline within 1–2 min. Under these conditions, neuronal damage failed to induce any DICTs. DICTs were also occluded in the presence of another P2Y receptor agonist, 2-MeSADP ($n = 6$, not shown). These data suggest that DICTs are mediated by ATP or its analogs acting on P2Y receptors.

Unfortunately, it was not possible to directly test this hypothesis using P2Y receptor antagonists because of the lack of potent, specific blockers. The drugs available (suramin (1 mM in the pipette, $n = 5$), RB-2 (reactive blue 2, 100 μM, $n = 5$), and PPADS (pyridoxal-5′-phosphate-6-azophenyl-2′,4′-disulfonic acid; 10 mM, $n = 5$)) failed to block DICTs even when applied directly to the microglial cell of interest (see Materials and methods for details), with drug application beginning at least 1 min before damaging the neuron.

Therefore, we tested whether DICTs require Ca^{2+} release from the intracellular Ca^{2+} stores, as would be expected for signals mediated by P2Y receptors. To do so we locally applied thapsigargin. Thapsigargin causes irreversible blockade of endoplasmic reticulum Ca^{2+} pumps and thereby empties intracellular Ca^{2+} stores [51,52]. As expected, thapsigargin application caused a complete blockade of responses to the agonist of metabotropic $P2Y_6$ receptors UDP, whereas responses to Bz-ATP, preferentially activating ionotropic $P2X_7$ receptors, were still present (Fig. 5C, D). Under these experimental conditions, DICTs were also completely blocked ($n = 4$, Fig. 5D). We concluded, therefore, that DICTs critically depend on Ca^{2+} release from the intracellular Ca^{2+} stores.

4. Discussion

Other than morphological studies [3,4,53–56], little is known about functional properties of differentiated (surveillant) microglia. This is mostly due to technical difficulties caused by the fact that (i) these cells have to be studied *in vivo* and (ii) the commonly used technique for *in vivo* labeling of cells with calcium indicator dyes [23] does not label microglia (Supplementary Fig. 1). Here we describe an approach enabling *in vivo* analyses of Ca^{2+} signaling in differentiated microglia. It combines *in vivo* labeling of the tissue with Isolectin B4 conjugated to Alexa Fluor 594 (or the use of genetically modified animals with fluorescently labeled microglia), single-cell electroporation technique, and high-resolution two-photon calcium imaging and can be used for analyses of microglial function in non-modified, wild-type mice.

So far, our knowledge about *in vivo* function of microglia comes mostly from CX_3CR1 mice [3,4,55]. Despite a small concern regarding a decreased level of fractalkine receptor expression in these animals [22], it is generally accepted that microglia in $CX_3CR1^{+/GFP}$ mice behave like wild-type microglia [50]. Consistently, a recent study using Iba1-eGFP mice reported very similar kinetics of microglial process motility in both mouse strains [54]. The *in vivo* IB4-based labeling technique introduced here allows to visualize microglia in any deliberate mouse strain. This approach abandons time-consuming crossing of mouse lines and thus significantly accelerates studies in which multiple cell types have to be fluorescently labeled (e.g., [54]). IB4 binds to α-D-galactose-containing glycoconjugates on the surface of microglial cells [31,32] and was previously mostly used as a postmortem histological marker. Although theoretically IB4 binding can impact on the functional properties of labeled microglial cells, our data suggest that this is not the case. Indeed, both eGFP- and IB4-AF594-labeled microglial cells had (i) similar chemotactic responses, (ii) similar kinetics of ATP-induced intracellular Ca^{2+} transients, and (iii) reliably responded with large Ca^{2+} transients to a focal damage of a nearby neuron. In addition, microglial cells in both preparations had similar pharmacological profiles. Thus, the *in vivo* IB4-labeling protocol introduced here seems to be a useful tool for studying microglial function.

The approach described above enabled us to study *in vivo* Ca^{2+} signaling in differentiated surveillant microglia. Our data suggest that under physiological conditions, differentiated microglia are rather silent in terms of their Ca^{2+} signaling. Indeed, at rest ~80% of cells tested did not show a single Ca^{2+} transient during a 15-min-long recording period. Ca^{2+} transients in remaining cells were rare and were not correlated with spontaneous Ca^{2+} waves in surrounding astrocytes. This finding contrasts with the data obtained in rat hippocampal cultures [40]. In culture spontaneous Ca^{2+} transients in microglial cells are caused by ATP released from neighboring astrocytes. Astrocyte-released ATP activates $P2X_7$ receptors in microglia and can even trigger microglial apoptosis [40]. Although astrocytes generate spontaneous Ca^{2+} transients also *in vivo* (Fig. 2A, B) and microglia are equipped with highly sensitive ATP receptors (Fig. 4D–F), under resting conditions, astrocytic Ca^{2+} signals do not propagate to neighboring microglia. Interestingly, the incidence of spontaneous Ca^{2+} transients in microglia remained low even in conditions of strong neuronal activity (Fig. 2C). This led us to conclude that somatic Ca^{2+} signaling is not required for surveying function of microglia.

We hypothesized therefore that microglia undergo an increase in $[Ca^{2+}]_i$ not spontaneously but in response to disturbance of tissue homeostasis. Indeed, all microglial cells studied responded with large Ca^{2+} transients to focal damage of an individual neuron in their vicinity (Fig. 3). On the level of the individual microglial cell, this Ca^{2+} signal represented a generalized event. At the same time, it was strictly localized to the cells dwelling within a 50-μm vicinity of a damaged neuron. Interestingly, generation of rapid DICT signals is a feature unique to microglia. Astrocytes, although also equipped with ATP receptors [57], either did not respond to neuronal damage at all (60% of cells) or did so with a much longer delay (Supplementary Fig. 3).

Our data show that DICTs are caused by Ca^{2+} release from the intracellular Ca^{2+} stores. Two lines of evidence suggest that this Ca^{2+} release is triggered by activation of P2Y receptors: (i) spatial and temporal properties of DICTs are faithfully mimicked by local application of ATP (Figs. 1D, 4E), ATPγS (Fig. 5A), and UDP (Fig. 5B) and (ii) DICTs are occluded by ATPγS as well as agonists of metabotropic P2Y receptors UDP and 2-MeSADP. According to our functional data (Fig. 4) as well as receptor expression studies of others [58,59], DICTs are most likely to be mediated by $P2Y_6$ or $P2Y_1$ (eventually also $P2Y_{2/4}$) receptors. Unfortunately, the lack of potent non-competitive P2Y receptor blockers precluded the direct test of this hypothesis. The drugs available (suramin, RB-2, and PPADS) failed to block DICTs. This failure is not surprising because none of the drugs are a potent selective blocker of the listed above receptors [60–62]. In addition, *in vivo* pharmacology has several technical caveats. To be effective *in vivo* antagonists have to be applied in a concentration ~10 times higher than the one used in cell cultures or tissue slices [4,24].

This was not possible for suramin because of solubility issue, whereas prolonged applications of high concentrations of RB-2 (≥1 mM) destroyed surrounding tissue.

Therefore, as they stay now our data are also consistent with the possibility that DICTs are caused by an unknown substance acting via another type of metabotropic receptor, which in turn activates intracellular store-mediated Ca^{2+} release. However, this alternative seems less likely. Because DICTs occur very rapidly, this unknown substance has to be released from damaged neurons at the relatively high concentration and on the millisecond time scale. This is true for neuronal neurotransmitters, in the cortex mostly for glutamate. However, neither glutamate itself nor metabotropic receptor agonist trans-ACPD were able to activate 100% of cells tested. Other metabotropic receptor agonists (e.g., carbachol and oxotremorine) failed to cause any Ca^{2+} transients at all. Interestingly, although microglial cells *in vivo* also express functional P2X receptors (as indicated by Bz-ATP- and α-β-MeATP-induced Ca^{2+} signaling, Fig. 4), the ionotropic purinoreceptors are not involved in DICT generation.

The functional role of these long-lasting, generalized microglial Ca^{2+} signals remains to be explored. DICTs occur immediately after neuronal damage (on the millisecond-to-second scale) and thus long before the damage-induced changes in microglial morphology (initiated within the first few minutes [3,4]) take place. Therefore, DICTs most likely operate as a switch, triggering processes relevant to microglial activation. Such processes may include (i) reorganization of actin cytoskeleton [53,63,64], (ii) CREB phosphorylation [2,65], (iii) gene expression and *de novo* protein synthesis (e.g., production of cytokines and chemokines, cyclooxygenase-2 [1,6,65], and BDNF [5,66]), (iv) release of pro- and/or anti-inflammatory mediators [1,6,8], and (v) microglial phagocytosis [67]. The fact that DICTs remain restricted in space suggests that single-cell damage is treated as a local event, involving only immediately adjacent microglia.

Taken together, our data suggest that *in vivo* somatic Ca^{2+} signaling in microglia is not involved in the surveillance of the extracellular milieu or in the detection of physiological levels of neuronal/astroglial activity. Rather, it functions as highly sensitive and specific signal for recognition of the damage in the microglial microenvironment.

Supplementary materials related to this article can be found online at doi:10.1016/j.bbamcr.2010.10.018.

Acknowledgments

We thank A. Weible, S. Kasperek, G. Heck, K. Schoentag for technical assistance and A. Verkhratsky, A. Konnerth, and L.B. Cohen for comments on the manuscript. This work was supported by grants from the Deutsche Forschungsgemeinschaft (SFB 596, GA 654/1-1).

References

[1] U.K. Hanisch, H. Kettenmann, Microglia: active sensor and versatile effector cells in the normal and pathologic brain, Nat. Neurosci. 10 (2007) 1387–1394.
[2] R.M. Ransohoff, V.H. Perry, Microglial physiology: unique stimuli, specialized responses, Annu. Rev. Immunol. 27 (2009) 119–145.
[3] A. Nimmerjahn, F. Kirchhoff, F. Helmchen, Resting microglial cells are highly dynamic surveillants of brain parenchyma in vivo, Science 308 (2005) 1314–1318.
[4] D. Davalos, J. Grutzendler, G. Yang, J.V. Kim, Y. Zuo, S. Jung, D.R. Littman, M.L. Dustin, W.B. Gan, ATP mediates rapid microglial response to local brain injury in vivo, Nat. Neurosci. 8 (2005) 752–758.
[5] K. Inoue, Purinergic systems in microglia, Cell. Mol. Life Sci. 65 (2008) 3074–3080.
[6] J.G. McLarnon, Purinergic mediated changes in Ca^{2+} mobilization and functional responses in microglia: effects of low levels of ATP, J. Neurosci. Res. 81 (2005) 349–356.
[7] T. Möller, Calcium signaling in microglial cells, Glia 40 (2002) 184–194.
[8] K. Färber, H. Kettenmann, Functional role of calcium signals for microglial function, Glia 54 (2006) 656–665.
[9] L. Ohana, E.W. Newell, E.F. Stanley, L.C. Schlichter, The Ca^{2+} release-activated Ca^{2+} current (I(CRAC)) mediates store-operated Ca^{2+} entry in rat microglia, Channels (Austin) 3 (2009) 129–139.
[10] T. Moller, Calcium signaling in microglial cells, Glia 40 (2002) 184–194.
[11] E.C. Toescu, T. Möller, H. Kettenmann, A. Verkhratsky, Long-term activation of capacitative Ca^{2+} entry in mouse microglial cells, Neurosci. 86 (1998) 925–935.
[12] E.W. Newell, E.F. Stanley, L.C. Schlichter, Reversed Na^{+}/Ca^{2+} exchange contributes to Ca^{2+} influx and respiratory burst in microglia, Channels (Austin) 1 (2007) 366–376.
[13] T. Moller, O. Kann, A. Verkhratsky, H. Kettenmann, Activation of mouse microglial cells affects P2 receptor signaling, Brain Res. 853 (2000) 49–59.
[14] K. Inoue, Microglial activation by purines and pyrimidines, Glia 40 (2002) 156–163.
[15] A. Hoffmann, O. Kann, C. Ohlemeyer, U.K. Hanisch, H. Kettenmann, Elevation of basal intracellular calcium as a central element in the activation of brain macrophages (microglia): suppression of receptor-evoked calcium signaling and control of release function, J. Neurosci. 23 (2003) 4410–4419.
[16] K. Färber, H. Kettenmann, Purinergic signaling and microglia, Pflügers Arch. 452 (2006) 615–621.
[17] D.B. Re, S. Przedborski, Fractalkine: moving from chemotaxis to neuroprotection, Nat. Neurosci. 9 (2006) 859–861.
[18] Y.H. Cui, Y. Le, X. Zhang, W. Gong, K. Abe, R. Sun, J. Van Damme, P. Proost, J.M. Wang, Up-regulation of FPR2, a chemotactic receptor for amyloid beta 1–42 (A beta 42), in murine microglial cells by TNF alpha, Neurobiol. Dis. 10 (2002) 366–377.
[19] D. Cui, H. Kawano, M. Takahashi, Y. Hoshii, M. Setoguchi, T. Gondo, T. Ishihara, Acceleration of murine AA amyloidosis by oral administration of amyloid fibrils extracted from different species, Pathol. Int. 52 (2002) 40–45.
[20] T. Möller, O. Kann, A. Verkhratsky, H. Kettenmann, Activation of mouse microglial cells affects P2 receptor signaling, Brain Res. 853 (2000) 49–59.
[21] K. Färber, H. Kettenmann, Physiology of microglial cells, Brain Res. Brain Res. Rev. 48 (2005) 133–143.
[22] G.A. Garden, T. Möller, Microglia biology in health and disease, J. Neuroimmune Pharmacol. 1 (2006) 127–137.
[23] C. Stosiek, O. Garaschuk, K. Holthoff, A. Konnerth, In vivo two-photon calcium imaging of neuronal networks, Proc. Natl Acad. Sci. USA 100 (2003) 7319–7324.
[24] O. Garaschuk, R.I. Milos, C. Grienberger, N. Marandi, H. Adelsberger, A. Konnerth, Optical monitoring of brain function in vivo: from neurons to networks, Pflügers Arch. 453 (2006) 385–396.
[25] P. Flecknell, Laboratory Animal Anaesthesia, Academic Press, San Diego, 2000.
[26] R.F. Hoyt, J.V. Hawkins, M.B. St Clair, M.J. Kennett, Mouse physiology, in: J.G. Fox, S.W. Barthold, M.T. Davisson, C.E. Newcomer, F.W. Quimby, A.L. Snith (Eds.), The Mouse in Biomedical Research, Academic Press (Elsevier), Burlington, MA, USA, 2007, pp. 23–78.
[27] K. Sohya, K. Kameyama, Y. Yanagawa, K. Obata, T. Tsumoto, GABAergic neurons are less selective to stimulus orientation than excitatory neurons in layer II/III of visual cortex, as revealed by in vivo functional Ca^{2+} imaging in transgenic mice, J. Neurosci. 27 (2007) 2145–2149.
[28] H. Hirase, L. Qian, P. Bartho, G. Buzsaki, Calcium dynamics of cortical astrocytic networks in vivo, PLoS Biol. 2 (2004) E96.
[29] X. Wang, N. Lou, Q. Xu, G.F. Tian, W.G. Peng, X. Han, J. Kang, T. Takano, M. Nedergaard, Astrocytic Ca^{2+} signaling evoked by sensory stimulation in vivo, Nat. Neurosci. 9 (2006) 816–823.
[30] A. Nimmerjahn, F. Kirchhoff, J.N. Kerr, F. Helmchen, Sulforhodamine 101 as a specific marker of astroglia in the neocortex in vivo, Nat. Methods 1 (2004) 31–37.
[31] W.J. Streit, An improved staining method for rat microglial cells using the lectin from *Griffonia simplicifolia* (GSA I-B4), J. Histochem. Cytochem. 38 (1990) 1683–1686.
[32] W.J. Streit, G.W. Kreutzberg, Lectin binding by resting and reactive microglia, J. Neurocytol. 16 (1987) 249–260.
[33] T. Nevian, F. Helmchen, Calcium indicator loading of neurons using single-cell electroporation, Pflügers Arch. 454 (2007) 675–688.
[34] S. Nagayama, S. Zeng, W. Xiong, M.L. Fletcher, A.V. Masurkar, D.J. Davis, V.A. Pieribone, W.R. Chen, In vivo simultaneous tracing and Ca^{2+} imaging of local neuronal circuits, Neuron 53 (2007) 789–803.
[35] B. Judkewitz, M. Rizzi, K. Kitamura, M. Hausser, Targeted single-cell electroporation of mammalian neurons in vivo, Nat. Protoc. 4 (2009) 862–869.
[36] K. Kitamura, B. Judkewitz, M. Kano, W. Denk, M. Hausser, Targeted patch-clamp recordings and single-cell electroporation of unlabeled neurons in vivo, Nat. Methods 5 (2008) 61–67.
[37] O. Garaschuk, R.I. Milos, A. Konnerth, Targeted bulk-loading of fluorescent indicators for two-photon brain imaging in vivo, Nat. Protoc. 1 (2006) 380–386.
[38] S. Jung, J. Aliberti, P. Graemmel, M.J. Sunshine, G.W. Kreutzberg, A. Sher, D.R. Littman, Analysis of fractalkine receptor CX(3)CR1 function by targeted deletion and green fluorescent protein reporter gene insertion, Mol. Cell. Biol. 20 (2000) 4106–4114.
[39] R.D. Fields, G. Burnstock, Purinergic signalling in neuron–glia interactions, Nat. Rev. Neurosci. 7 (2006) 423–436.
[40] C. Verderio, M. Matteoli, ATP mediates calcium signaling between astrocytes and microglial cells: modulation by IFN-gamma, J. Immunol. 166 (2001) 6383–6391.
[41] C. Agulhon, J. Petravicz, A.B. McMullen, E.J. Sweger, S.K. Minton, S.R. Taves, K.B. Casper, T.A. Fiacco, K.D. McCarthy, What is the role of astrocyte calcium in neurophysiology? Neuron 59 (2008) 932–946.
[42] M.A. Busche, G. Eichhoff, H. Adelsberger, D. Abramowski, K.H. Wiederhold, C. Haass, M. Staufenbiel, A. Konnerth, O. Garaschuk, Clusters of hyperactive neurons

near amyloid plaques in a mouse model of Alzheimer's disease, Science 321 (2008) 1686–1689.
[43] T.H. Schwartz, T. Bonhoeffer, In vivo optical mapping of epileptic foci and surround inhibition in ferret cerebral cortex, Nat. Med. 7 (2001) 1063–1067.
[44] E. Sykova, C. Nicholson, Diffusion in brain extracellular space, Physiol. Rev. 88 (2008) 1277–1340.
[45] J.M. Pocock, H. Kettenmann, Neurotransmitter receptors on microglia, Trends Neurosci. 30 (2007) 527–535.
[46] E.R. Whittemore, A.R. Korotzer, A. Etebari, C.W. Cotman, Carbachol increases intracellular free calcium in cultured rat microglia, Brain Res. 621 (1993) 59–64.
[47] L. Zhang, J.G. McLarnon, V. Goghari, Y.B. Lee, S.U. Kim, C. Krieger, Cholinergic agonists increase intracellular Ca^{2+} in cultured human microglia, Neurosci. Lett. 255 (1998) 33–36.
[48] E.W. Boddeke, I. Meigel, S. Frentzel, K. Biber, L.Q. Renn, P. Gebicke-Harter, Functional expression of the fractalkine (CX3C) receptor and its regulation by lipopolysaccharide in rat microglia, Eur. J. Pharmacol. 374 (1999) 309–313.
[49] C.A. Colton, M. Jia, M.X. Li, D.L. Gilbert, K^+ modulation of microglial superoxide production: involvement of voltage-gated Ca^{2+} channels, Am. J. Physiol. 266 (1994) C1650–C1655.
[50] D.B. Re, S. Przedborski, Fractalkine: moving from chemotaxis to neuroprotection, Nat. Neurosci. 9 (2006) 859–861.
[51] O. Thastrup, P.J. Cullen, B.K. Drobak, M.R. Hanley, A.P. Dawson, Thapsigargin, a tumor promoter, discharges intracellular Ca^{2+} stores by specific inhibition of the endoplasmic reticulum Ca^{2+}-ATPase, Proc. Natl Acad. Sci. USA 87 (1990) 2466–2470.
[52] A. Gamberucci, B. Innocenti, R. Fulceri, G. Banhegyi, R. Giunti, T. Pozzan, A. Benedetti, Modulation of Ca^{2+} influx dependent on store depletion by intracellular adenine-guanine nucleotide levels, J. Biol. Chem. 269 (1994) 23597–23602.
[53] D.J. Hines, R.M. Hines, S.J. Mulligan, B.A. Macvicar, Microglia processes block the spread of damage in the brain and require functional chloride channels, Glia 57 (2009) 1610–1618.
[54] H. Wake, A.J. Moorhouse, S. Jinno, S. Kohsaka, J. Nabekura, Resting microglia directly monitor the functional state of synapses in vivo and determine the fate of ischemic terminals, J. Neurosci. 29 (2009) 3974–3980.
[55] S.E. Haynes, G. Hollopeter, G. Yang, D. Kurpius, M.E. Dailey, W.B. Gan, D. Julius, The P2Y12 receptor regulates microglial activation by extracellular nucleotides, Nat. Neurosci. 9 (2006) 1512–1519.
[56] L.J. Wu, K.I. Vadakkan, M. Zhuo, ATP-induced chemotaxis of microglial processes requires P2Y receptor-activated initiation of outward potassium currents, Glia 55 (2007) 810–821.
[57] A. Verkhrasky, O.A. Krishtal, G. Burnstock, Purinoceptors on neuroglia, Mol. Neurobiol. 39 (2009) 190–208.
[58] F. Bianco, M. Fumagalli, E. Pravettoni, N. D'Ambrosi, C. Volonte, M. Matteoli, M.P. Abbracchio, C. Verderio, Pathophysiological roles of extracellular nucleotides in glial cells: differential expression of purinergic receptors in resting and activated microglia, Brain Res. Brain Res. Rev. 48 (2005) 144–156.
[59] A.R. Light, Y. Wu, R.W. Hughen, P.B. Guthrie, Purinergic receptors activating rapid intracellular Ca increases in microglia, Neuron Glia Biol. 2 (2006) 125–138.
[60] I. von Kugelgen, Pharmacological profiles of cloned mammalian P2Y-receptor subtypes, Pharmacol. Ther. 110 (2006) 415–432.
[61] I. von Kugelgen, Pharmacology of mammalian P2x- and P2y-receptors, Biotrend Rev. 9 (2008) 1–11.
[62] V. Ralevic, G. Burnstock, Receptors for purines and pyrimidines, Pharmacol. Rev. 50 (1998) 413–492.
[63] T.G. Oertner, A. Matus, Calcium regulation of actin dynamics in dendritic spines, Cell Calcium 37 (2005) 477–482.
[64] M. Cristofanilli, A. Akopian, Calcium channel and glutamate receptor activities regulate actin organization in salamander retinal neurons, J. Physiol. 575 (2006) 543–554.
[65] Y.D. Potucek, J.M. Crain, J.J. Watters, Purinergic receptors modulate MAP kinases and transcription factors that control microglial inflammatory gene expression, Neurochem. Internat. 49 (2006) 204–214.
[66] A.E. West, E.C. Griffith, M.E. Greenberg, Regulation of transcription factors by neuronal activity, Nat. Rev. Neurosci. 3 (2002) 921–931.
[67] S. Koizumi, Y. Shigemoto-Mogami, K. Nasu-Tada, Y. Shinozaki, K. Ohsawa, M. Tsuda, B.V. Joshi, K.A. Jacobson, S. Kohsaka, K. Inoue, UDP acting at P2Y6 receptors is a mediator of microglial phagocytosis, Nature 446 (2007) 1091–1095.